Final Report

for Award DE-SC0005403: Improved Electrochemical Performance of Strained Lattice Electrolytes via Modulated Doping

funded by the Department of Energy
Office of Basic Energy Sciences
Division of Materials Sciences and Engineering

Program Manager:
Dr. Bonnie Gersten
Division of Materials Sciences & Eng., SC-22.2
Germantown Building
1000 Independence Avenue, SW
Washington, DC 20585-1290
301-903-0002 (ph)
Bonnie.Gersten@science.doe.gov

Principal Investigator:
Ajay Prasad

University of Delaware
210 Hullihen Hall
Newark, DE 19716

Sep 6, 2015

Executive Summary

The ultimate goal of this project was to learn how to systematically strain the inter-atomic distance in thin ceramic films and how to use this newfound control to improve the ease by which oxygen ions can conduct through the films. Increasing the ionic conductivity of ceramics holds the promise of drastic improvements in the performance of solid oxide fuel cells, chemical sensors, gas permeation membranes, and related devices. Before this work, the experimental evidence advocating for strain-based techniques was often controversial and poorly characterized. Enabling much of this work was a new method to quickly create a very wide range of ceramic nanostructures that was established during the first phase of the project. Following this initial phase, we created a variety of promising nanostructured epitaxial films and multilayers with systematic variations in lattice mismatch and dopant content.

Over the course of the work, a positive effect of tensile atomic strain on the oxygen conductivity was conclusively found using a few different forms of samples and experimental techniques. The samples were built by sputtering, an industrially scalable technique, and thus the technological implementation of these results may be economically feasible. Still, two other results consistently achieved over multiple efforts in this work give pause. The first of these results was that very specific, pristine surfaces upon which to build the nanostructures were strictly required in order to achieve measurable results. The second of these results was that *compressively* strained films with concomitant *reductions* in oxygen conductivity are much easier to obtain relative to tensile-strained films with increased conductivity.

Comparison of the Actual Accomplishments with the Goals and Objectives of the Project

The work accomplished nearly all of the initial goals and objectives of this project, and made important discoveries in areas not initially anticipated as well. The initial goals listed in the proposal were to:

- systematically create strained lattice oxide ion electrolyte multilayers by sputtering ZrO_2 and CeO_2 based films with spatially modulated dopant and host atom concentrations and performing detailed structural and chemical characterization, including determination of coherence strain in the layers as a function of layer thickness and dopant and host atom concentrations;
- determine the effects of the strained lattices on ionic conductivity and surface exchange in cubic fluorite oxide solid electrolytes using impedance spectroscopy; and
- find methods, such as HEMT-like structures, to use nanometric multilayers of conventional materials to improve low temperature oxygen ion conductivity and surface exchange rates, ultimately leading to improved performance of SOFCs and other devices based on solid electrolytes.

By the end of the first year of the project, the ability to sputter ZrO_2 and CeO_2 based films with spatially modulated dopant and host atom concentrations was fully met, as described in detail in publications 2 and 7 (numbered as listed at the end of this report). Importantly, heteroepitaxy of these films was achieved without the use of $SrTiO_3$ (STO) buffer layers. Such buffer layers are commonly used in the literature, but have been shown to significantly confuse subsequent electrical measurements. Detailed structural and chemical characterization of these films is described in publications 2 and 7 as well, using cross-sectional high resolution transmission electron microscopy (TEM), x-ray diffraction (XRD), and depth-profiling secondary ion mass spectroscopy (SIMS). The results of various diffraction techniques used to characterize the coherency strains are discussed in publications 4, 7, 9, 11, 12, & 14.

During the remainder of the project, these sputtering and characterization methods were used to systematically study YSZ and GDC thin films and nanostructured multilayers in order to ascertain the effects of strained lattices on ionic conductivity. An example of these findings are that thicker (≥50 nm)

YSZ films deposited on c-plane sapphire exhibited a conductivity similar to bulk samples, but thinner films (< 10 nm) obtained a conductivity 0.5–1.5 orders of magnitude higher. As the thickness decreased from 100 to 6 nm, X-ray diffraction showed that the out-of-plane lattice parameter increased from 5.21 to 5.24 Å. More systematic study came from multilayers where the lattice mismatch was systematically controlled. In these studies (largely discussed in publications 12 and 14), it was conclusively found that each 1% increase in compressive strain in yttria-doped ceria yields a 1.6-fold reduction in interfacial conductivity at 650 °C and a 3-fold reduction at 450 °C. However, the multilayers also showed that YSZ could not support tensile strains of ≈ 1.5% or more, and thus the ability to increase conductivity in this way is limited.

Promising non-conventional multilayer structures for improved conductivity with controlled, mesoscale ordering of the dopant atoms were explored and are described in publications 6 and 11. It was found first that significant ion conduction could be supported in the space charge zone near the interfaces of pure ceria and pure dopant-oxide. A Guoy-Chapman model of interfacial conduction was shown to successfully capture much of the measured sample behavior. Continued research showed that strain in this space charge zone, as induced by the lattice mismatch with different rare earth oxides used as the hetero-dopant, controlled the activation energy of conduction. With the benefit of conduction through tensile-strained, highly pure ceria space charge regions, the conductivity of CeO_2-La_2O_3 films measured in this work approached that of highly optimized, homogeneously doped ceria systems.

Project Activities for the Entire Period of Funding

This project advanced fairly closely along the schedule originally proposed. The stated goal for the first year was to determine suitable deposition conditions for films from which multilayers will be built. Sputtering targets for Ce, Zr, Y, and Gd were sourced and procedures for using these materials, some of which were magnetic and/or pyrophoric, were settled. Calibration depositions were performed on silicon substrates to determine deposition rates for the pure oxides under a range of typical deposition conditions. Importantly, conditions were found that support deposition rates from the host atoms, Zr and Ce, that range from about 1x to 10x that from the dopant atoms, Gd and Y. This range is exactly what was needed to obtain dopant concentrations that ranged from about 10% up to 50%.

Following on this, series of zirconia-yttria (YSZ), ceria-gadolinia (GDC), ceria-yttria (YDC) and ceria-zirconia (CZO) films with ranges of solid solution compositions were fabricated. As shown in Figure 1, a deviation was found between the expected atomic ratio derived from the previous deposition rate calibrations and the actual atomic ratio measured by EDS. Specifically, the actual atomic ratio was increased over the expected atomic ratio by a factor of 1.38 for YSZ, 1.49 for GDC, and nearly 1 for CZO. The compositions of a few of the samples were corroborated by XPS to ensure that this effect was not merely a measurement artifact of the EDS.

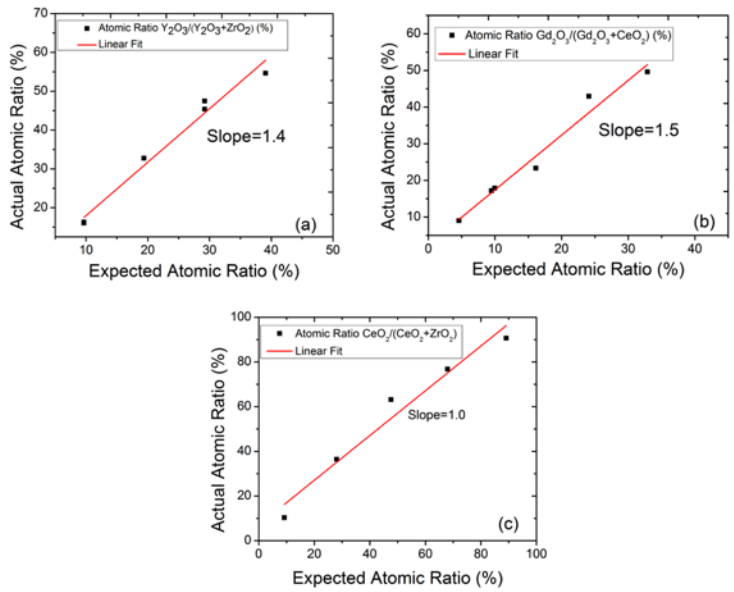

Figure 1. The relationship between the expected atomic ratio and the actual atomic ratio in deposition of (a) YSZ, (b) GDC, and (c) CZO.

Having proven the ability to make films of arbitrary composition, both (100) MgO and (0001) Al_2O_3 were tested as substrates for epitaxial growth. 75-nm thick films with composition $Zr_{0.85}Y_{0.15}O_{2-\delta}$ and $Ce_{0.8}Gd_{0.2}O_{2-\delta}$ were tested to represent the extremes of lattice parameter to be examined in this work. Figure 2 shows the XRD patterns of these films. Whereas YSZ exhibited a very high degree of (100) orientation when deposited on the MgO substrates, GDC exhibited weak peaks along multiple axes, indicative of randomly oriented, nanocrystalline grains. Both films were highly oriented along the (111) direction when deposited on the Al_2O_3 substrates. Electron diffraction shown in Figure 3 verified that the initial YSZ films were epitaxial on MgO with a cube-on-cube orientation. Based on the electron diffraction pattern, the lattice mismatch was largely relaxed. This is likely due to a high concentration of planar dislocations at the interface.

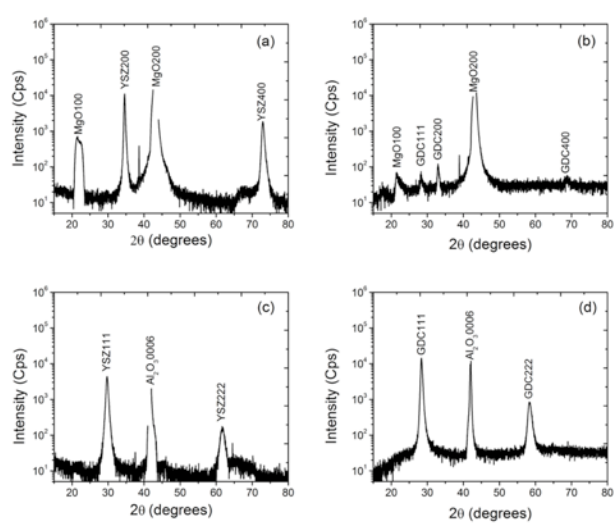

Figure 2. θ-2θ XRD patterns of initial (a) YSZ and (b) GDC films deposited on (100) MgO and (c) YSZ and (d) GDC films deposited on (0001) Al_2O_3. Note that the intensity scale is logarithmic.

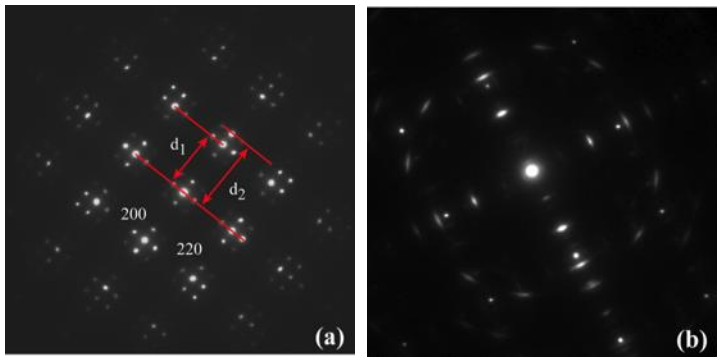

Figure 3. Plan view SAED pattern of YSZ (a) and GDC (b) deposited on (100) MgO substrate.

The GDC directly deposited on (100) MgO was poorly textured (Figure 2b). To see if the highly textured YSZ could be used as a buffer layer for textured GDC film growth on (100) MgO, a multilayer of YSZ and GDC films was fabricated. The GDC was deposited on the top surface of YSZ, as shown in the inset of Figure 4. The films were each approximately 75 nm thick. According to the diffraction pattern in Figure 4, both films in this sample were highly oriented along the (100) direction. Thus, the intermediate lattice parameter of YSZ—between that of MgO and GDC—allows the use of YSZ as a buffer layer for oriented GDC film growth. Fabricating epitaxial GDC films without a STO buffer layer prevents any conductivity related to the STO buffer layer from affecting the electrical measurement of the heterostructure films.

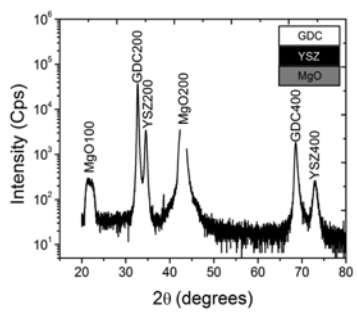

Figure 4. θ-2θ XRD patterns of bilayer film of GDC and YSZ deposited on (100) MgO. A sketch of the heterostructure is shown in the inset.

The initial plan was that thin films fabricated in this work would be electrochemically characterized using both impedance spectroscopy and isotope exchange. Isotope exchange is not often performed using thin films, so a natural question becomes what values of oxygen ion diffusivity (*D*) and surface exchange coefficient (*k*) are measurable using them. Thin samples require a more generalized solution to the diffusion equation than typically used in order to understand the ionic motion within the material during isotope exchange. Through rigorous numerical analysis of the more complex analytical model that results, we determined the conditions when *k* and/or *D* can be measured using both thin film and traditional samples. Characteristic parameters related to the exchange time (*t*), material thickness (*l*), *D*, and *k* were derived to quantify these conditions. The conventional idea that *k* can be measured when $\frac{l \cdot k}{D} < 1$ whereas *D* can be measured when $\frac{l \cdot k}{D} > 1$ was found to be correct but incomplete. Indeed, simultaneous measurement of *k* and *D* is possible using samples of any thickness, provided that, among a few other constraints, $5 \cdot 10^{-6} \leq \frac{k^2 \cdot t}{D} \leq 20$. An example result from this work is shown in Figure 5. Experimental verification of these findings using isotope exchange measurements of sputtered $LaCoO_3$ and $SrCoO_3$ films was performed.

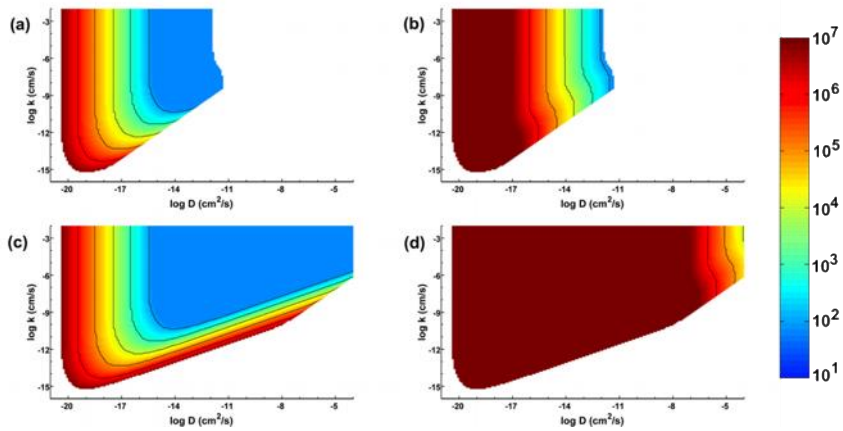

Figure 5. Contour plot of the minimum (a and c) and maximum (b and d) practical isotope exchange time that can be used to measure *D* using a 100 nm thick film (a and b) or 1 cm thick sample (c and d). Values are plotted as a function of *k* and *D*. The time value in seconds is indicated by shade, keyed to the bar on far right. Black lines within the plots indicate contour levels at $t = 10^2$ s, 10^3 s, 10^4 s, 10^5 s, and 10^6 s.

Having proven the ability to make epitaxial films of ceria, zirconia, and ceria-zirconia with arbitrary host atom ratio and dopant composition, the simplest means to test the effect of lattice strain on ionic conduction comes from measuring nanoscale, single layer thin films. Yttria-stabilized zirconia (YSZ) thin films with thickness ranging from 6 nm to 100 nm were prepared by RF sputtering on (0001) Al_2O_3 substrates and, as shown in Figure 6, exhibited epitaxial growth along YSZ (111)[110] // Al_2O_3 (0001)[$10\bar{1}0$]. While the thicker films exhibited oxygen ion conductivities similar to bulk samples, figure 7 shows that the thinnest films exhibited increased ionic conductivity and a reduced activation energy of 0.79 eV between 300 °C – 650 °C. Concomitant with the improved conductivity of the thinner films was an increase in the out-of-plane lattice parameter, matching theoretical expectations regarding tensile strain, and the introduction of edge dislocations, which may additionally assist in-plane ionic conduction.

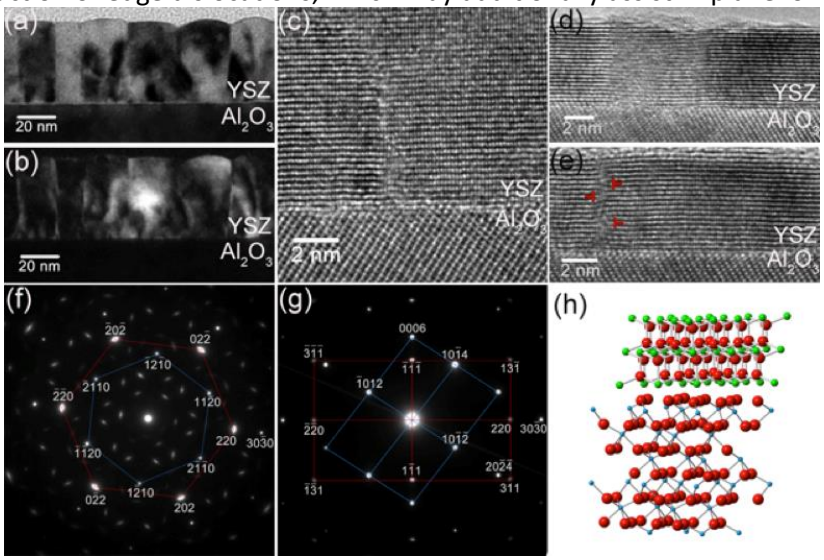

Figure 6. (a) Bright-field, (b) dark-field, and (c) high resolution cross-sectional image of a 50 nm thick, as-deposited YSZ thin film. (d) High resolution image of 6 nm thick YSZ thin film as-deposited and (e) after high temperature impedance measurements. Red marks indicate edge dislocations. (f) In-plane and (g) cross-section electron diffraction of 50 nm thick as-deposited YSZ thin films and (h) solid sphere model of YSZ/Al_2O_3 interface. Green, blue, and red spheres represent Zr/Y, Al, and O, respectively.

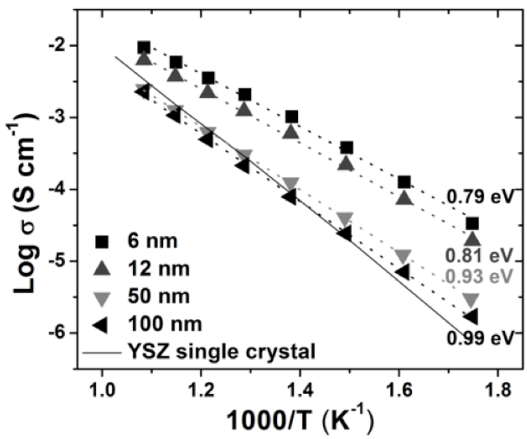

Figure 7. Arrhenius plot of the conductivity of the 9 mol% YSZ thin films as well as a single crystal YSZ substrate with nominally similar composition. Activation energies listed for the films are calculated from the σ·T product.

For comparison, nanoscale 20 mol% gadolinia-doped ceria (GDC) thin films were prepared by RF sputtering on single crystal (0001) Al_2O_3 substrates. The films were polycrystalline with columnar grains that were very highly textured along the (111) direction. A moderate amount of lattice strain was observed when the thickness was less than 81 nm, similar to the grain size. Impedance spectroscopy measurements between 300 °C and 650 °C demonstrated that GDC thin films achieved highest conductivity at 81 nm thickness (Figure 8). The activation energy was ≈ 0.75 eV when thickness was under 81 nm but increased as the thickness increased above 81 nm. Constant conductivity values for all samples as the oxygen partial pressure varied between 10^{-3} atm and 1 atm demonstrated that the conductivity was predominantly ionic.

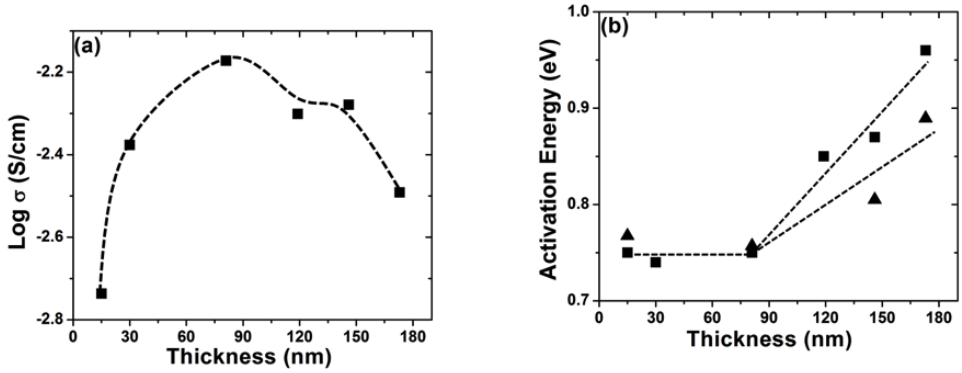

Figure 8. The thickness dependence of the (a) conductivity at 500 °C and (b) activation energy of the σ·T product of GDC films. Squares and triangles represent fresh and annealed samples, respectively.

A promising heterostructure discussed in the proposal was the HEMT-analog, where film layers with high defect concentration are situated next to more pure layers with high defect mobility. In the past year, we fabricated and characterized Y-doped CeO_2 thin films where the Y dopants were distributed homogeneously or were condensed into increasingly concentrated layers, to the limit of alternating layers of pure Y_2O_3 and pure CeO_2. Schematic pictures of the samples are shown in figure 9 and high-resolution TEM cross sections are shown in figure 10. Both the entire film thickness and net Y-concentration were kept constant such that only the spatial distribution of dopants was altered. Space charge regions formed at interfaces between regions with varying vacancy concentrations, yielding vacancies trapped within two-dimensionally arranged accumulation regions.

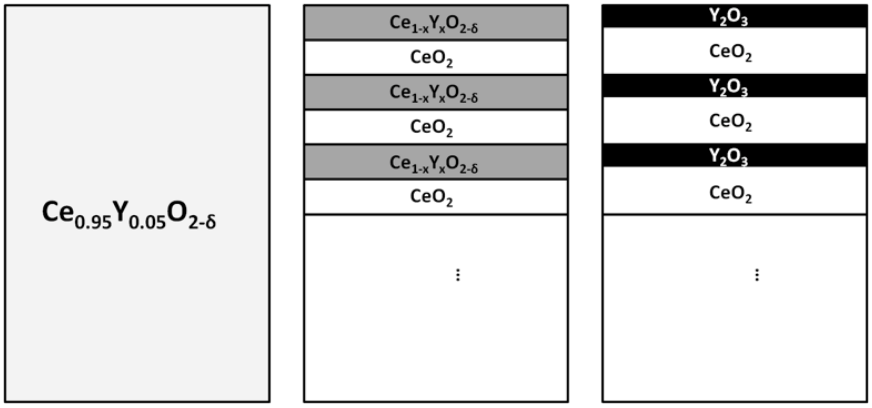

Figure 9. Schematic diagram of the structures of $Ce_{0.95}Y_{0.05}O_{2-\delta}$ films with modulated composition. The Y-dopant concentration *x* in $Ce_{1-x}Y_xO_{2-\delta}$ layers is gradually increased while keeping the net Y-dopant concentration of the whole film at a constant 5% by adjusting the relative thickness ratio between CeO_2 and Y-containing layers. Total film thickness was kept constant at ≈ 200 nm.

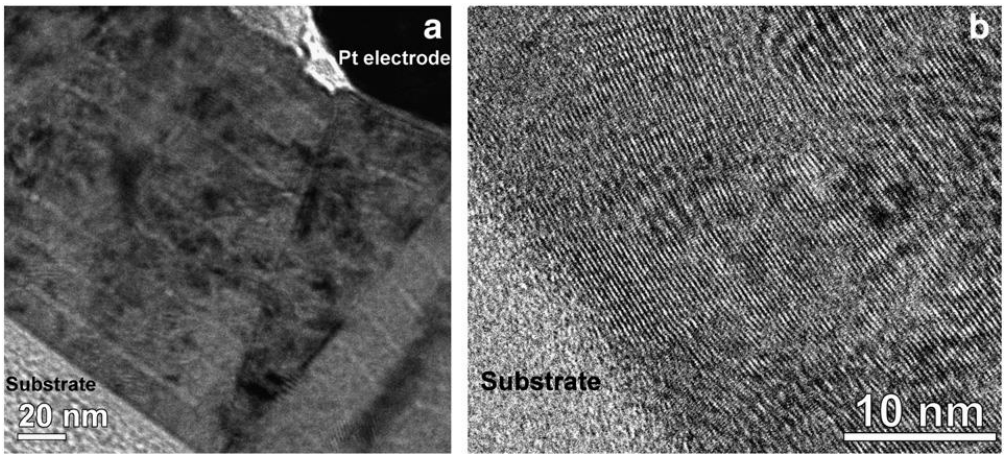

Figure 10. (a) Bright field TEM cross section of a sample like the one shown at right in Figure 9. Bright stripes of 1 nm thick Y_2O_3 are clearly visible against darker, 19 nm thick CeO_2 regions. A grain growing at an off-angle is visible right-of-center. In addition to the film, the substrate and platinum electrode are visible. (b) High resolution TEM of a near-substrate portion of the film cross section.

Impedance spectra were collected for the samples over a range of temperatures (figure 11a and 11b). A Gouy-Chapman model was implemented in order to further investigate the distribution of the accumulated oxygen vacancies in the space charge regions of pure CeO_2 layers. Comparison of the measured activation energy of conduction (figure 11c) indicates that in films with intermediate dopant condensation, conduction occurred predominantly by vacancies trapped in the Y-containing layers. Conversely, in the film composed of alternating layers of Y_2O_3 and CeO_2, vacancies trapped in the CeO_2 space charge regions became significantly conductive, thus providing a new experimental means to determine the properties of vacancies in ceria that are trapped near dopants.

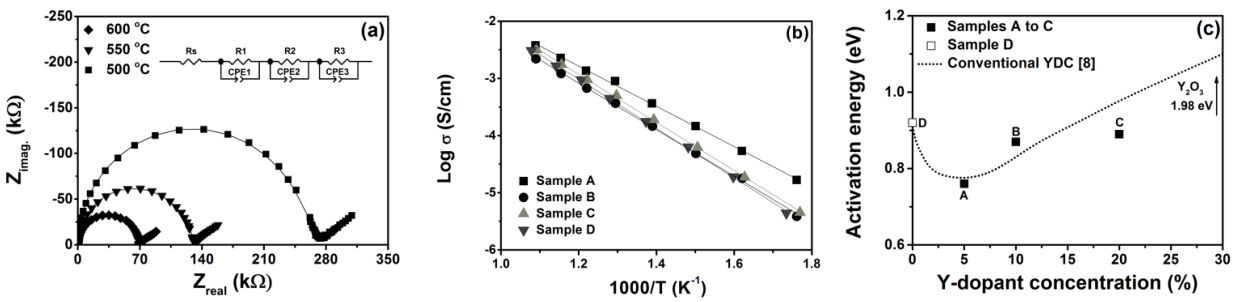

Figure 11. (a) Impedance spectra of the sample shown on the right in figure 4 (sample 'D') at the temperatures indicated and the equivalent circuit used to fit the data. (b) Arrhenius plots of electrical conductivities measured for all samples, and (c) the activation energy of the σ·T product of the samples as a function of the Y-dopant concentration in the Y-containing layer. Sample D is plotted at zero dopant concentration because evidence and theory suggest that the mobile defects are trapped in space charge regions in the pure CeO_2 layers. Also shown for reference is the activation energy of conventionally fabricated YDC samples as reported in the literature and pure Y_2O_3 as calculated from oxygen diffusion measurements reported in the literature.

Expanding on this work, the effects of lattice mismatch strain on heterogeneously doped ceria was studied using films with alternating layers of CeO_2 with 1 nm thick dopant oxides of Y_2O_3, Gd_2O_3, or La_2O_3. The classical Gouy–Chapman model used to explain the results in figure 11 was found to no longer be sufficient to fully explain the ion conduction behavior of these heterodoped films. Gouy-Chapman theory predicts identical conductivity for these three dopants, however these were not the results obtained experimentally (figure 12). Instead, the film conductivity increased with increasing lattice parameter of the dopant. Two effects of the lattice mismatch were suggested. First, compressive strain in CeO_2 decreased the oxygen vacancy mobility in Y_2O_3/CeO_2 films, as evidenced by an increased activation energy of conduction. Second, strain gradients at the interfaces were suggested to cause more oxygen vacancies to be transferred into the CeO_2 space charge regions in the La_2O_3/CeO_2 films. Further investigations in this area are merited by the fact that the conductivity of these heterogeneously doped systems was already approaching the conductivity of optimal homogeneously doped systems. Taking advantage of strain gradients and high net dopant content in heterogeneously doped materials may indicate a route to significantly increase solid electrolyte conductivity over what is achievable with traditional doping strategies.

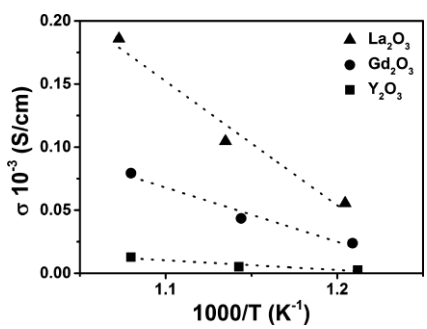

Figure 12. Conductivity per CeO_2-R_2O_3 heterodopant interface, obtained from the slope of the linear fit of the conductivity as a function of the number of interfaces.

The most direct demonstrations of the goals of this work came in two studies at the end of the project that examined multilayer structures where undoped CZO layers with varying cerium/zirconium ratio were used to change the lattice mismatch strain applied to interleaved YSZ or YDC layers. Since the lattice parameter of CZO is highly dependent on the Ce/Zr atomic ratio, its use enables precise control of

the strain magnitude in neighboring lattice planes of YDC. In the first study, multilayers composed of YDC and CZO allowed systematic quantification of the effect of biaxial compressive strain. Detailed x-ray diffraction analysis showed that the lattice mismatch was accommodated by elastic strain. Three series of multilayers were fabricated using $Ce_{0.55}Zr_{0.45}O_2$ (CZO45), $Ce_{0.70}Zr_{0.30}O2$ (CZO30), and CeO_2, with an interfacial lattice mismatch of ≈2.2%, ≈1.5%, and near-zero, respectively. The compressive strain in the YDC layers caused fairly drastic reductions in the ionic conductivity. Figure 13 shows that each 1% increase in compressive strain in the YDC yielded a 1.6-fold reduction in interfacial conductivity at 650 °C and a 3-fold reduction at 450 °C. Other interfacial effects, however, were also found to have significant impact on the ionic conduction.

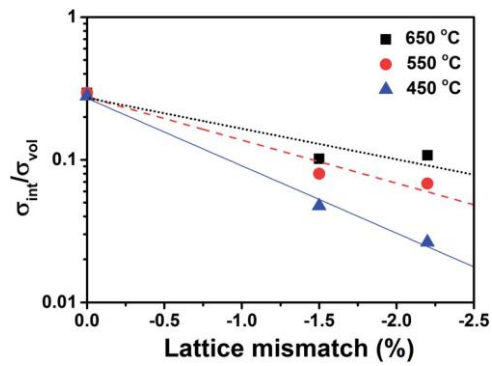

Figure 13. The interfacial conductivity (normalized to the volume conductivity) of YDC/CZO multilayers as a function of the lattice mismatch. The negative slope indicates reduced conductivity with increasing biaxial compression.

In the final study performed in this work, thin film multilayers composed of 9 mol% YSZ and CZO were used to systematically quantify the effects of tensile strain on the oxygen-ion conduction behavior in YSZ. The same three sets of CZO layers were used as with the previous study: CeO_2, CZO30, and CZO45. These layers provided the YSZ with interfacial lattice mismatch values of +5.2%, +3.7%, and +2.9%, respectively. When decreasing the individual layer thicknesses from 35 nm to 5 nm, none of the multilayers exhibited any significant change of the conductivity, with values consistently near that of bulk YSZ (figure 14). X-ray diffraction results indicated that the interfacial strains were largely relaxed, most likely from dislocation nucleation at the interfaces.

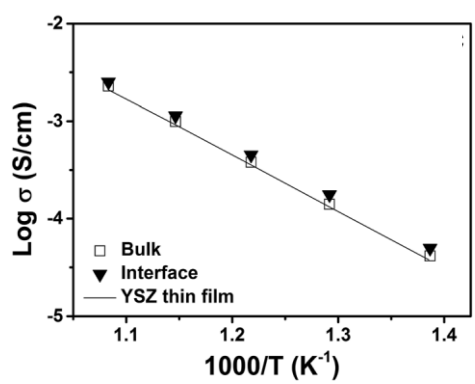

Figure 14. An Arrhenius plot of the bulk and interfacial conductivities of a YSZ/CZO45 multilayer. The lack of a difference between the two conductivities indicate no interfacial effect in this multilayer.

Products developed under the award and technology transfer activities:

Publications:

1. E. Fischer, J.L. Hertz, "Measurability of the diffusion and surface exchange coefficients using isotope exchange with thin film and traditional samples," *Solid State Ionics*, **218**, p. 18 (2012)
2. J. Jiang, W. Shen, J.L. Hertz, "Fabrication of epitaxial zirconia and ceria thin films with arbitrary dopant and host atom composition," *Thin Solid Films*, **522**, p. 66 (2012)
3. E. Fischer, W. Shen, J.L. Hertz, "Measurement of the surface exchange and diffusion coefficients of thin film $LaCoO_3$ and $SrCoO_x$," *J. Electroceramics*, **29**, p. 262 (2012)
4. J. Jiang, X. Hu, W. Shen, C. Ni, J.L. Hertz, "Improved ionic conductivity in strained yttria-stabilized zirconia thin films," *Appl. Phys. Lett.*, **102**, 143901 (2013)
5. J. Jiang, W. Shen, J.L. Hertz, "Structure and ionic conductivity of nanoscale gadolinia-doped ceria thin films," *Solid State Ionics*, **249-250**, p. 139 (2013)
6. W. Shen, J. Jiang, C. Ni, Z. Voras, T.P. Beebe, J.L. Hertz, "Two-dimensional vacancy trapping in yttria-doped ceria," *Solid State Ionics*, **255**, p. 13 (2014)
7. J. Jiang, D. Clark, W. Shen, J.L. Hertz, "The effects of substrate surface structure on yttria stabilized zirconia thin films," *Appl. Surf. Sci.*, **293**, p. 191 (2014)
8. J. Jiang, J.L. Hertz, "Intermediate temperature surface proton conduction on dense YSZ thin films," *J. Mater. Chem. A*, **2**, p. 19550 (2014)
9. J. Jiang, X. Hu, N. Ye, J.L. Hertz, "Microstructure and ionic conductivity of yttria-stabilized zirconia thin films deposited on MgO," *J. Am. Ceram. Soc.*, **97**, p. 1131 (2014)
10. J. Jiang, J.L. Hertz, "On the variability of reported ionic conductivity in nanoscale YSZ thin films," *J. Electroceramics*, **32**, p. 37 (2014)
11. W. Shen, J.L. Hertz, "Beneficial lattice strain in heterogeneously doped ceria," *J. Phys. Chem. C*, **118**, p. 22904 (2014)
12. W. Shen, J. Jiang, J.L. Hertz, "Reduced ionic conductivity in biaxially compressed ceria," *RSC Adv.*, **4**, p. 21625 (2014)
13. W. Shen, J. Jiang, J.L. Hertz, "Using thin films to investigate heterogeneous defect chemistry," *J. Electroceramics*, **34**, p. 74 (2015)
14. W. Shen, J.L. Hertz, "Ionic conductivity of YSZ/CZO multilayers with variable lattice mismatch," *J. Mater. Chem. A*, **3**, p. 2378 (2015)

Talks:

1. J.L. Hertz, "Multilayer Films for Solid Oxide Fuel Cell Electrolytes," *Composites at Lake Louise*, Oct. 30, 2011
2. W. Shen, J. Jiang, J.L. Hertz "Structural characterization of epitaxial fluorite thin films," *Materials Research Society 2011 Fall Meeting*, Nov. 29, 2011
3. J. Jiang, W. Shen, J.L. Hertz, "The fabrication and electrochemical properties of strained YSZ/GDC thin films," *Materials Research Society 2011 Fall Meeting*, Nov. 28, 2011
4. J. Jiang, "Fabrication and Electrochemical Properties of Strained Zirconia and Ceria Thin Films," *Materials Research Society 2012 Fall Meeting*, Nov. 28, 2012
5. W. Shen, "Determination of the Role of Strain on Oxygen Ion Conductivity in Epitaxial Zirconia and Ceria Multilayers," *Materials Research Society 2012 Fall Meeting*, Nov. 26, 2012
6. J. L. Hertz, "Epitaxial Zirconia and Ceria Based Thin Films and Multilayers with Arbitrary Composition," *The Electrochemical Society 2012 Fall Meeting*, Oct. 8, 2012

7. J. L. Hertz, “Nanoengineered Model Systems for Solid Oxide Fuel Cells,” *American Chemical Society National Meeting*, Apr. 11, 2013
8. J. L. Hertz, “Using thin films to investigate heterogeneous (defect) chemistry,” *The 19th International Conference on Solid State Ionics*, June 7, 2013
9. J. L. Hertz, “Heterogeneous thin films to model and improve solid electrolytes,” *Princeton University Department of Mechanical and Aerospace Engineering Seminar*, Feb. 21, 2014